Transition metal compounds with S/N-functionalized NHC ligands: structures, redox properties and electrocatalytic activity

Luo, S.; Luo S.

CHAPTER 3

Nickel Complexes of Pyridine-Functionalized N-heterocyclic Carbenes: Syntheses, Structures, and Activity in Electrocatalytic Hydrogen Production

*Two bis-(benz)imidazolium salts alkylated with pyridyl side arms, H_2**L1**Br_2 (1,2-bis[(1-(2-pyridylmethyl)-benzimidazolium-3-yl)-methyl]benzene bromide) and H_2**L2**Br_2 (1,2-bis[(1-(2-pyridylmethyl)-imidazolium-3-yl)-methyl]benzene bromide) have been prepared and were used as precursors in the synthesis of novel nickel compounds of N-heterocyclic carbenes (Ni-NHC). The four Ni-NHC complexes [Ni(**L1**)Br]Br (**1a**), [Ni(**L1**)]$(PF_6)_2$ (**1b**), [Ni(**L2**)]Br_2 (**2a**) and [Ni(**L2**)]$(PF_6)_2$ (**2b**) were isolated and characterized by various methods, and the X-ray crystal structures of **1a**, **2a** and **2b** are reported. The nickel ion in **1a** is in a square-pyramidal geometry with one of the bromide ions in the apical position, the nickel ions in **2a** and **2b** are in square-planar geometries. The compounds of the ligand with an imidazole-based carbene revealed much higher activity in electrocatalytic proton reduction and better acid tolerance, although their overpotentials are higher than those of the benzimidazole-based compounds. The presence of bromide ions has an adverse effect on the redox potentials as well as the overpotentials for proton reduction. Complex **2b**, having the most planar coordination geometry, appeared to have the highest catalytic efficiency for proton reduction in DMF (i_c/i_p = 50, k_{obs} = 490 s^{-1} at 0.1 V/s) when using acetic acid as the proton source.*

This chapter has been published as a full paper: S. Luo, M.A. Siegler, E. Bouwman, Eur. J. Inorg. Chem. **2016**, 2016, 4693-4700.

3.1 Introduction

Dihydrogen is an environmentally friendly energy carrier as upon combustion it only produces H_2O.[1, 2] In order to enable the establishment of a society based on dihydogen as an energy source, for many years researchers have focused on the search for efficient proton-reduction catalysts, notably for catalysts that are not based on noble metals.[3-7] In the field of bioinorganic chemistry the synthesis of structural models of hydrogenases is a common strategy to devise molecular catalysts for proton reduction.[8, 9] However, the so-called 'functional models' of hydrogenases, which do not exhibit exactly similar structures, appear to result in more active and more stable catalytic systems. The two-electron donor ligands such as phosphanes and amines have been widely used in combination with Co[10-12] and Ni[7, 13] metal centers. The N-heterocyclic carbene (NHC) ligand is also a two-electron donor, with strong binding properties comparable to that of phosphane ligands.[14] Although Ni-NHC complexes have found various applications in organometallic chemistry,[15-21] the electrocatalytic properties of this kind of compounds so far mostly have been neglected.

NHC ligands functionalized with pyridine groups have been used to synthesize nickel and palladium complexes that were found to be efficient catalysts for the Kumada cross-coupling[22] and Heck-type coupling reactions.[23] Recently, the group of Kubiak reported a study of nickel compounds with four carbene ligands including their electrochemical characterization, but their activity in electrocatalysis was not discussed.[24] A series of nickel N-heterocyclic carbene-pyridine complexes was reported by Thoi *et al*.[25, 26] to selectively reduce carbon dioxide to carbon monoxide. Nevertheless, the number of studies in the area of electrocatalysis using Ni-NHC compounds is limited. In this Chapter, we report four novel Ni-NHC complexes obtained with the ligand precursors H_2**L1**Br_2 and H_2**L2**Br_2, which are based on bis(benz)imidazolium salts bridged by a xylyl linker (Figure 3.1). We have studied their redox properties and electrocatalytic activity for proton reduction in an organic solvent.

3.2 Results and Discussion

3.2.1 Synthesis of complexes

The two bis(benz)imidazolium salts 1,2-bis[(1-(2-pyridylmethyl)-benzimidazolium-3-yl)-methyl]benzene bromide (H_2**L1**Br_2) and 1,2-bis[(1-(2-pyridylmethyl)-imidazolium-3-yl)-methyl]benzene bromide (H_2**L2**Br_2) were synthesized following published procedures with small modifications (details in chapter 3.4).[27, 28] The nickel bromide compounds [Ni(**L1**)Br]Br (**1a**) and [Ni(**L2**)]Br_2 (**2a**) were obtained as yellow-colored powders from a melt of nickel acetate with the ligand in tetrabutylammonium bromide (TBAB) in good yields (74% and 55%, respectively). The color of complex **1a** turned to orange once dried under vacuum overnight. Whereas the benzimidazole-based complex **1a** is poorly soluble in water, the imidazole-based compound **2a** is soluble in water. Compounds **1b** and **2b** were obtained from **1a** and **2a** via anion exchange by adding a solution of the complex in

methanol to a boiling methanol solution of NH_4PF_6. All complexes are air and moisture stable in the solid state for at least several months. The low-spin character of the Ni^{II} ion in all compounds is evidenced by their diamagnetic ^1H NMR spectra, indicating that the square-planar geometry of the Ni centers is retained in solution. The ESI-MS analysis of the four compounds shows the presence of monocationic (with one coordinated bromide anion, or as an ion pair) as well as dicationic fragment ions. Recrystallized samples of the Ni compounds were dried in vacuo before elemental analysis was performed; however, the results still show the presence of the corresponding solvents that were used in recrystallization.

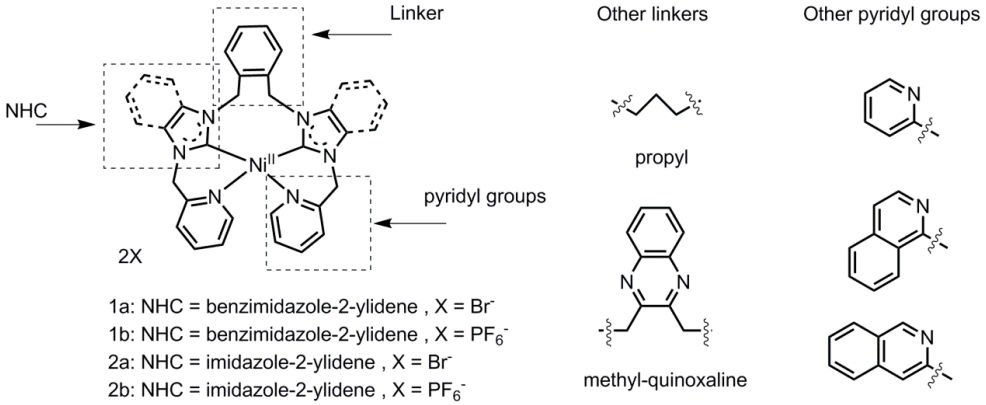

Figure 3.1. Complexes reported in this paper (linker = xylyl) and related compounds previously reported (with linker = propyl[26] or methyl-quinoxaline[29]).

3.2.2 Structural characterization of the complexes

Single crystals of **1a**, **2a**, and **2b** suitable for X-ray diffraction were obtained using the liquid-liquid diffusion method (MeCN/ether). The crystallographic data are provided in Table AIII.1; selected bonds lengths and bond angles are given in Table 3.1.

Compound **1a** crystallizes as a monocationic complex with one uncoordinated bromide ion and 1.5 water molecules per asymmetric unit. The nickel ion in complex **1a** is coordinated in a square-pyramidal geometry, with the donor atoms of the tetradentate ligand in the equatorial plane and one coordinating bromide ion at the apical position (Figure 3.2). The bond distance to the apical bromide (Ni1–Br2) is 3.0800(8) Å. This distance is rather long and could be considered as a normal van der Waals contact; however, also the coordination angles (between 86 - 99°), the small torsion angle of the equatorial plane and the low τ_5 value (see below) are indicative of a stronger interaction. The tetradentate ligand is wrapped around the nickel ion with the aromatic groups orientated in a zig-zag fashion with respect to each other. The ligand donor atoms form an approximate plane with only a small torsion angle (N22-N52-C42-C12 = 5.18(8)°), with Ni–N and Ni–C bond lengths in the range of 1.882 – 1.963 Å, consistent with the typical distances reported for this type of structures.[21, 29] The N–Ni–C and C–Ni–C bond angles are slightly smaller than the ideal

right angles (87.42 – 88.86°), but the 'open' N52–Ni1–N22 angle is slightly larger (95.85(9)°). The 5-coordinate geometry is characterized with a τ_5 value of 0.09, indicating that the nickel ion is coordinated in a near ideal square pyramid.[30]

The five-coordinate geometry of the nickel ion in **1a** is not rare; 5-coordinated geometries can be divided into two categories: the trigonal bipyramid[31] and the tetragonal pyramid.[32] The square-pyramidal geometry is commonly formed with pentadentate chelating ligands,[33] or from a combination of tridentate and bidentate chelating ligands.[34, 35] Square-pyramidal structures formed by a tetradentate ligand with an additional halide ion are rather rare.[36, 37] The non-coordinating bromide ion and the lattice water molecules are connected with the coordinating bromide ion via hydrogen bonding interactions.

Compounds **2a** and **2b** crystallize as dicationic complexes with the non-coordinating bromide ions and the solvent molecules (**2a**) or the hexafluoridophosphate ions (**2b**) in the crystal lattice. The nickel ion in these complexes is coordinated in a square-planar geometry, with the donor atoms of the tetradentate ligand wrapped around the nickel ion (Figure 3.2). The Ni–N bond lengths in **2a** and **2b** are slightly shorter than those in **1a**, whereas the Ni–C bond distances are rather similar (Table 3.1).

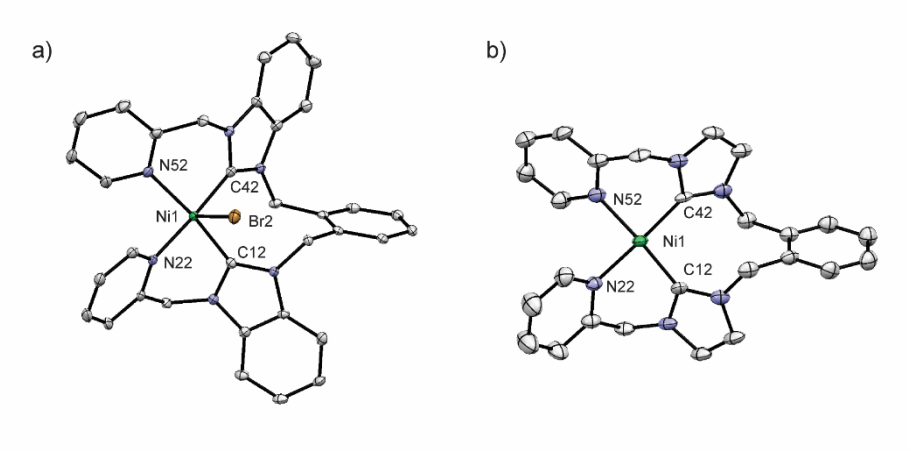

*Figure 3.2. Displacement ellipsoid plots (50% probability level) of the cations: a) [Ni(**L1**)Br]$^+$ in **1a** and b) [Ni(**L1**)]$^{2+}$ in **2b** at 110(2) K. Atom numbering scheme for the first coordination sphere is provided. Hydrogen atoms, the non-coordinated bromide ion, the hexafluoridophosphate ion and the lattice water molecules are omitted for clarity.*

The square-planar geometry of the nickel ion in **2a** was evaluated with an equation[24] derived from a report by Yang:[38]

$$\tau_4 = \frac{360-(\alpha+\beta)}{2\alpha}\delta;\ \delta = \frac{\beta}{\alpha}$$

The largest (α) and second-largest (β) L–Ni–L angles in **2a** are 171.7(3) and 167.7(2)°, resulting in a τ_4 value of 0.06. For compound **2b**, a τ_4 value of 0.04 is calculated,

indicating that the geometry of the central ion in both compounds is close to the ideal square-planar geometry. The structures of the nickel(II) compounds have been compared with those earlier reported (Table 3.1 and Table AIII.2);[26] it appears that ligands containing pyridylmethyl pendant arms result in nickel(II) compounds with longer Ni─C bond distances than ligands with pyridyl side groups. The donor atoms of tetradentate ligands containing the more flexible pyridylmethyl groups are arranged in a more planar fashion around the nickel ions with lower τ_4 values (τ_4 = 0.09 for pyridylmethyl groups and 0.14 for pyridyl groups). The different linkers in the dicarbene chelating structure may also affect the planarity of the arrangement of donor atoms around the nickel centers. Ligands with rigid linkers containing an aromatic group such as xylene (**2a** τ_4 = 0.06; **2b** τ_4 = 0.04) or dimethylquinoxaline[29] (τ_4 = 0.03) present smaller τ_4 values than the ligands with alkyl linkers (τ_4 = 0.12~0.14, see Table AIII.2).[26]

*Table 3.1. Selected bond distances (Å) and angles (°) of compounds **1a**, **2a**, and **2b**.*

	1a	**2a**	**2b**
Ni1–N22	1.962(2)	1.946(7)	1.942(3)
Ni1–N52	1.963(2)	1.929(2)	1.932(3)
Ni1–C12	1.879(2)	1.877(5)	1.879(4)
Ni1–C42	1.882(2)	1.876(3)	1.887(4)
Ni1–Br2	3.080(8)		
N22-Ni1-C12	87.42(9)	87.29(3)	87.8(2)
N22-Ni1-C42	176.72(9)	171.7(3)	172.7(1)
N22-Ni1-N52	87.86(8)	86.5(3)	89.4(1)
C12-Ni1-C42	95.8(1)	99.1(2)	95.0(2)
C12-Ni1-N52	171.03(9)	167.7(2)	173.4(2)
C42-Ni1-N52	88.86(9)	88.2(1)	88.5(1)

3.2.3 UV-vis absorption studies

Electronic absorption spectroscopy of the four nickel compounds as well as the precursor ligands H_2**L1**Br_2 and H_2**L2**Br_2 was performed both in the solid state and in DMF solutions (see Table 3.2 and Figure AIII.3-4).

Table 3.2. Parameters of the electronic spectra of Ni complexes and ligands.

	Solid state optical spectra (nm)	Absorption bands, λ_{max} nm (ε/$M^{-1}cm^{-1}$)[a]
1a	264, 305, 355, 433sh	276 (2540), 285 (5000), 303 (5680), 312 (6140), 361sh (1040)
1b	262, 298, 324, 390	280 (4450), 314 (5860), 389sh (360)
2a	260, 308, 351	274 (4000), 305 (4860), 378sh (1950)
2b	258, 299, 384, 556sh	273 (2860), 307 (3860), 381sh (180)
H_2L1Br_2	259	275 (3220)
H_2L2Br_2	258	267 (2370)

The solid-state absorption spectra of the ligand precursors H_2**L1**Br_2 and H_2**L2**Br_2 show one absorption around 260 nm ascribed to π-π* transitions of the pyridyl groups.[39] The absorption bands in the solid-state spectrum of **1a** at 305 and 355 nm are assigned to ligand-to-metal charge-transfer (LMCT) transitions, and the absorption at 433 nm is assigned to a d-d transition. Similar assignments are proposed for the spectra of the other compounds (Figure AIII.3).

Compounds **2a**, **1b** and **2b** readily dissolve in dry DMF resulting clear (pale) yellow solutions (within 1 min). However, the solubility of **1a** is lower, initially resulting in a cloudy solution; only after stirring for 1 h the solution became clear. The limited solubility of **1a** in DMF may be related to the coordination of one of the bromide ions; perhaps only upon dissociation of this bromide ion the compound is fully soluble. The UV-Vis spectra in DMF again show the intense π-π* transition of the pyridyl groups at around 275 nm and an intense transition around 310 nm, which has been ascribed to a ligand-to metal charge transfer (LMCT of carbene to nickel).[40] All compounds show a d-d transition in the region of 360 – 380 nm common for square-planar nickel(II) complexes (Figure AIII.4).

3.2.4 Redox properties of Ni complexes

Electrochemical analysis of the four nickel complexes in dry DMF was performed with 0.1 M tetrabutylammonium hexafluoridophosphate (TBAP) as the supporting electrolyte under a stream of argon. An Ag/AgCl reference electrode was used, ferrocene was added at the end of each measurement as an internal standard. The potentials reported in this chapter are versus the ferrocene/ferrocinium ($Fc^{0/+}$) couple. The electrochemical data of the nickel compounds are collected in Table 3.3.

The cyclic voltammogram of complex **1a** shows the presence of three reductive waves, two of which are reversible (Figure 3.3). The two reversible waves are tentatively assigned to the Ni^{II}/Ni^{I} and Ni^{I}/Ni^{0} redox couples ($E_{1/2}$ = −1.55 V and −1.80 V). However, the formation of a Ni(I) species with a ligand-centred radical is also possible, although the voltammogram of the ligand does not have a reduction wave coinciding with the second reversible reduction of the complex. Without a full spectro-electrochemical study the true nature of the reduction process occurring at –1.8 V is unknown. The first reversible redox wave at −1.55 V vs $Fc^{0/+}$, is characterized by a peak current ratio i_{pa}/i_{pc} of 0.99. A plot of the reductive peak current i_{pc} displays a linear relationships with the square root of the scan rate (Figure AIII.5), which demonstrates this first electrochemical reduction to be diffusion-controlled.[41] In addition, the current also increases linearly with the concentration of the nickel compound (Figure AIII.5). The third small reductive peak at −2.04 V is tentatively attributed to a ligand-based process, forming a ligand-centered radical, as its position coincides with a peak observed in the CV of H_2**L1**Br_2 (Figure 3.3).

Compound **2a** reveals a similar cyclic voltammogram with three reduction processes at −1.76, −1.96 and −2.27 V, and two oxidation processes at −1.67 and −1.86 V. However, the redox processes are significantly less reversible; the peak-current ratio i_{pa}/i_{pc} of the first

reduction event is 0.75 indicating a quasi-reversible redox process (Figure AIII.6). The voltammograms of the hexafluoridophosphate species **1b** and **2b** show similar patterns compared to their bromide analogs, but with the redox processes occurring at less negative redox potentials (~20 to 50 mV); the presence of the potentially coordinating anions apparently stabilizes the Ni(II) oxidation state.

It appears that the nickel compounds with a benzimidazole-based carbene ligand are more readily reduced with less negative half-wave potentials (−1.53 V ~ −1.55 V) than those with the imidazole-based carbenes (−1.66 V ~ −1.71 V), indicating the imidazole-based ligands to be slightly more electron donating. The redox potentials of these nickel compounds with the relatively hard pyridyl ligands occur at rather negative potentials compared to Ni centers that are coordinated with softer phosphane ligands.[13, 32]

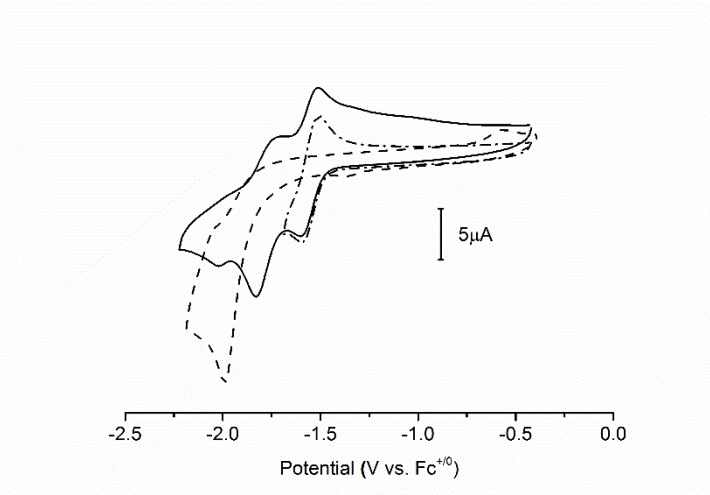

*Figure 3.3. Cyclic voltammograms of **1a** (1 mM, solid line and dash-dotted line) and H_2**L1**Br_2 (1 mM, dashed line) recorded in DMF in different scan ranges. Conditions: scan rate = 0.1 V/s, TBAP (0.1 M), glassy-carbon working electrode.*

Table 3.3. Electrochemical data of the nickel compounds.[a]

	E_{pc1} [V]	E_{pa1} [V]	$E_{1/2}$ [V] (ΔE_p [mV])	E_{pc2} [V]	E_{pa2} [V]	$E_{1/2}$ [V] (ΔE_p [mV])	E_{pc3} [V]
1a	−1.59	−1.51	−1.55 (82)	−1.84	−1.76	−1.80 (79)	−2.04
1b	−1.58	−1.49	−1.53 (84)	−1.80	−1.72	−1.76 (80)	−2.00
2a	−1.76	−1.67	−1.71 (82)	−1.96	−1.86	−1.91 (100)	−2.27
2b	−1.70	−1.63	−1.66 (75)	−1.90	−1.82	−1.86 (84)	−2.23

[a] All voltammograms were recorded in DMF; the potentials are referenced to the $Fc^{+/0}$ couple. Conditions: scan rate = 0.1 V/s, compound (1 mM), TBAP (0.1 M), glassy-carbon working electrode. Under these conditions we found $\Delta E_p(Fc^{+/0})$ = 78 mV.

3.2.5 Catalytic activity for proton reduction in non-aqueous solution

The four compounds have been investigated for their catalytic activity in the electrocatalytic proton reduction in DMF, using either acetic acid (HOAc) or trifluoroacetic acid (Htfa) as the proton source. For each scan the working electrode was freshly polished.

When using the acid Htfa as the proton source (pKa in DMF = 6.0[42]), two new reductive waves (−1.9 V and −2.4 V) appeared after two irreversible peaks at −1.6 V and −1.8 V (Figure 3.4a), consistent with the report of Canaguier *et al*.[6] The catalytic current i_c is the maximum current of the catalytic proton-reduction peak, and i_p is the plateau current of the non-catalytic reduction waves. The current of the catalytic wave is dependent on the acid concentration, but saturates at a concentration of 40 mM (Figure AIII.7). This saturation indicates that at this acid level the main rate-controlling process is no longer acid diffusion, but rather the catalytic efficiency of the Ni complex. In addition, in the acid-dependent region, the i_c/i_p ratio increases linearly with the square root of the acid concentration (Figure 3.4b). The i_c/i_p value is 43 in the acid-independent region (at a scan rate of 0.1 V/s) which corresponds to a rate constant (k_{obs}) of 360 s^{-1}.[7, 43]

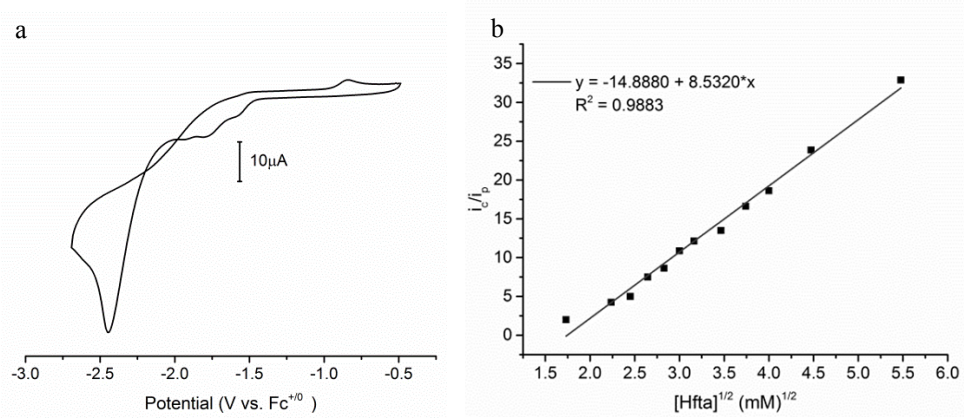

*Figure 3.4. (a) Cyclic voltammogram of **1a** (1 mM) in presence of Htfa (10 mM) recorded in DMF. (b)* Plot of i_c/i_p vs. $[Htfa]^{1/2}$ $(mM)^{1/2}$ for ***1a*** in presence of various concentrations of acid in DMF, *Conditions: scan rate = 0.1 V/s, TBAP (0.1 M), glassy-carbon working electrode.*

Activity for proton reduction is also observed when the weaker acetic acid is added to a solution of **1a** in DMF. The two reversible redox couples as well as the third irreversible reductive wave combine into one irreversible wave at −1.8 V. Meanwhile only one new reduction peak is observed at −2.6 V. The current of this peak is dependent on the acid concentration; this behavior is ascribed to the electrocatalytic reduction of protons by the nickel compound. The appearance of bubbles on the glassy carbon working electrode during the experiment is another visible indication for H_2 production. No obvious current enhancement is observed in a blank experiment using the same quantity of acid in the absence of nickel complex (see Figure AIII.8). The other three analogous nickel compounds show similar CVs in presence of acid: with the sequential addition of the acid,

the reductive current gradually increased (Figure 3.5). Moreover, we observed an acid-independent region after 20 mM acid for the benzimidazole-based compounds **1a** and **1b**.

In case of such similar structures those four compounds have, we initially assumed a first-order or pseudo-first order H_2 evolving reaction happened in the solution. Comparison of the catalytic activity of the four Ni complexes using acetic acid as the proton source revealed that the i_c/i_p value of compound **2b** is the highest, reaching 50 (corresponding to k_{obs} = 490 s^{-1} at 0.1 V/s) at an acid concentration of 80 mM (Table 3.4). The overpotential for electrocatalytic proton reduction at an acetic acid concentration of 10 mM of the four molecular catalysts has been calculated taking homoconjugation of the acid into account (Table 3.4).[44] The imidazole-based complex **2b**, which is the most efficient electrocatalyst of the four compounds, unfortunately displays a higher overpotential (1.28 V) than the benzimidazole-based carbene complexes (~1.15 V). Furthermore, the presence of bromide ions in complexes **1a** and **2a** results in slightly higher overpotentials (30 ~ 50 mV difference).

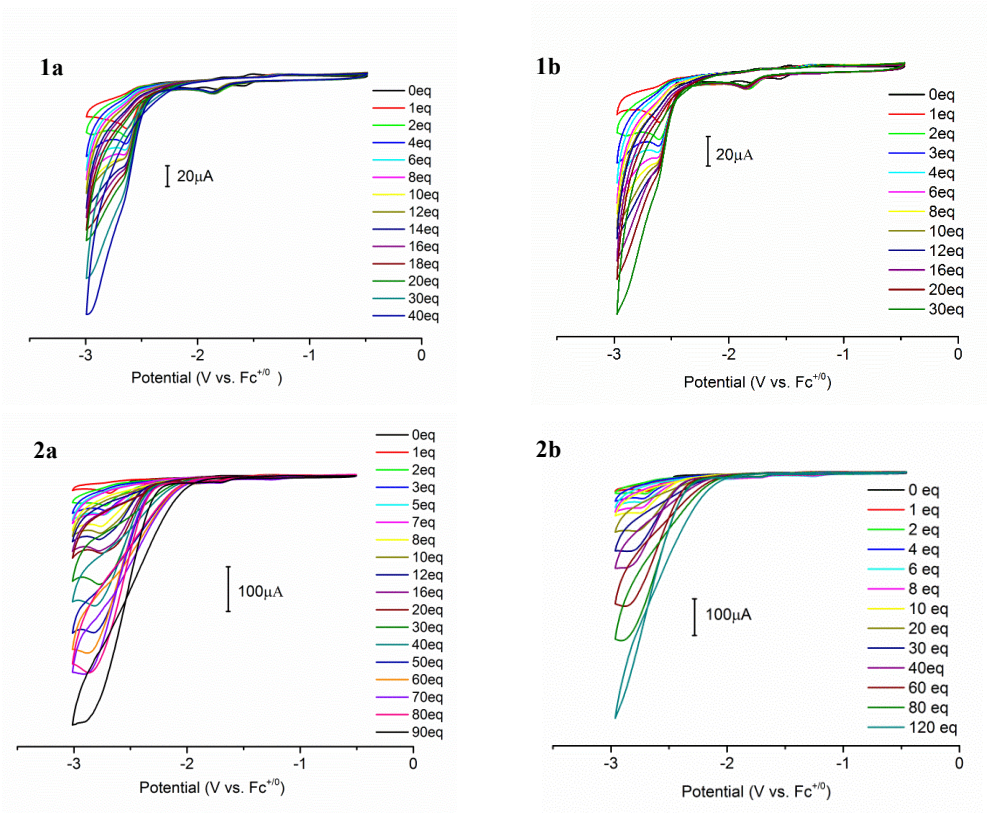

*Figure 3.5. The CVs of complexes **1a**, **1b**, **2a** and **2b** recorded in presence of various equivalents of acetic acid in DMF containing 0.1 M TBAP as supporting electrolyte at scan rate 0.1 V/s, using a glassy carbon working electrode.*

Table 3.4. Summary of the electrocatalytic properties of the compounds.[a]

	1a	**1b**	**2a**	**2b**
[HOAc] (mM)	16	16	80	80
i_c/i_p	11	9	40	50
k_{obs}	25	16	310	490
Overpotential (V)[b]	1.17	1.14	1.33	1.28

[a] The i_c/i_p value, k_{obs} and overpotentials of the reductive waves of the four complexes(1 mM) at the maximum concentration of acetic acid at a scan rate of 0.1 V/s (vs. $Fc^{+/0}$). [b] Overpotentials of proton reduction catalyzed by the complexes were calculated in the presence of 10 mM acetic acid.

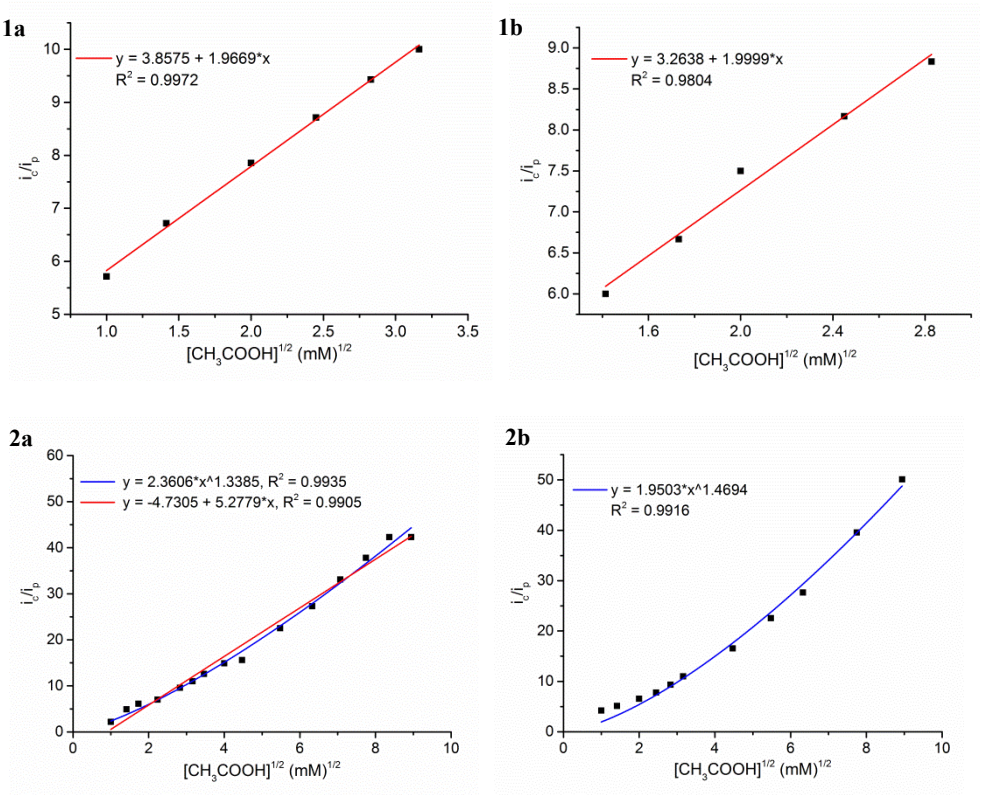

*Figure 3.6. Plots of i_c/i_p vs. $[CH_3COOH]^{1/2}$ $(mM)^{1/2}$ for four complexes (**1a** to **2b**) in presence of various acid concentration in DMF containing 0.1 M TBAP as supporting electrode at 0.1 V/s, using glassy carbon working electrode.*

The large difference in catalytic activity between the benzimidazole-based nickel-carbene compounds and the imidazole-based nickel-carbene compounds might be due to the difference in electron-donating properties of the ligands. The more electron-donating ligand based on imidazole results in better catalytic efficiency of its nickel compounds, but at the expense of larger overpotentials for proton reduction. Plots of the catalytic current i_c/i_p versus the square root of the acid concentration at the acid-dependent region (Figure 3.6) reveal a large difference in correlation between the benzimidazole-based species (**1a**, **1b**) and the imidazole-based compounds (**2a**, **2b**). For compounds **1a** and **1b** plots of i_c/i_p versus

the acid concentration in the acid-dependent region show a linear relationship, indicating that the reaction is first-order with respect to proton concentration.[7, 13, 32, 43, 45, 46] However, for compounds **2a** and **2b**, especially **2b**, the correlation between i_c/i_p versus $[H^+]^{½}$ is less linear. Especially for compound **2b**, which can be regarded as the best electrocatalyst of the four, a plot of i_c/i_p gives a linear relationship with acid concentration, instead of with square root of acid concentration (Figure 3.7). This relationship indicates that in the case of **2b**, two protons are involved in the rate-determining step of the reaction. Based on these data we propose that the rate-determining step in the catalytic mechanism of the benzimidazole-based species may be different from that of the imidazole-based compounds, which may also affect the efficiency of the catalysts. However, a DFT study needs to be carried out in order to understand the relationship between the catalyst's structure and its mechanism in detail.

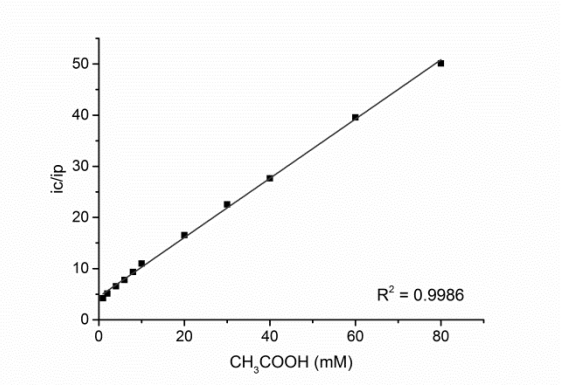

*Figure 3.7. Plots of i_c/i_p vs. [CH_3COOH] (mM) for complex **2b** in presence of various acid concentration in DMF containing 0.1 M TBAP as supporting electrode at 0.1 V/s, using a glassy carbon working electrode.*

3.3 Conclusion

In this chapter we report four novel pyridine-functionalized Ni-NHC complexes and their redox and electrocatalytic properties. The type and length of the linker between the carbenes as well as to the pyridine group influences the geometry of the complexes, as characterized by their τ_4 values. It appears that a rigid linker based on an aromatic group in combination with a methylenepyridine pendent group attributes to more ideal square-planar geometries. In addition, we found that the use of imidazole-based carbenes result in more negative Ni^{II}/Ni^{I} and Ni^{I}/Ni^{0} redox couples, although these compounds revealed much higher catalytic activity in electrocatalytic reduction of protons, as well as better acid tolerance. The most planar complex **2b** (with the smallest τ_4 value) shows the highest catalytic efficiency ($i_c/i_p = 50$, $k_{obs} = 490$ s^{-1} at 0.1 V/s) of all complexes investigated in this study for the catalytic proton reduction using acetic acid, although the overpotential at which dihydrogen is produced is sizeable. To the best of our knowledge, these are the first Ni-NHC complexes reported to catalyze proton reduction. Only a few recent reports relate to proton reduction with metal-NHC compounds, but these concern cobalt-NHC complexes.[14, 47] Furthermore, it was shown that the presence of halide ions results in more

negative potentials for the Ni^{II}/Ni^{I} and Ni^{I}/Ni^{0} redox couples, and also leads to larger overpotentials for proton reduction.

The experiments of catalytic proton reduction in organic solvents provide a starting point for analysis; however, water is the ideal solvent for H_2 production. Considering the higher solubility of the hexafluoridophosphate salts in aqueous solutions and the adverse effect of the bromide ions on the catalytic activity of the nickel compounds, further investigations to proton reduction catalysis with this type of molecular catalysts will be carried out in acid-buffered aqueous solutions. Although the observed overpotentials are not outstanding, the reported nickel compounds are attractive: the synthesis route of the complexes is straightforward and the complexes are air and moisture stable due to the presence of the bis-carbene donor.

3.4 Experimental

3.4.1 Materials

Commercial chemicals were used without further purification. Acetonitrile, tetrahydrofuran, dichloromethane and diethyl ether were obtained from a PureSolv MD5 solvent dispenser. Dry dimethylformamide was prepared by adding molecular sieves into commercial anhydrous solvent. The rest commercial solvents were used without further purification. *N*-Pyridylmethyl(benz)imidazole was synthesized following literature methods.[27] All air-sensitive reactions were performed under argon using standard Schlenk techniques unless mentioned otherwise.

3.4.2 Analytical methods

^{1}H, ^{13}C and ^{31}P NMR spectra were recorded on a Bruker 300 DPX spectrometer. Mass spectra were obtained using a Finnigan Aqua Mass Spectrometer (MS) with electro spray ionization (ESI). UV-vis spectra were obtained using either a transmission dip probe or a solid-state reflection probe on a Avantes Avaspec-2048 spectrometer with a Avalight-DH-S-BAL light source. Elemental analyses were performed by the Kolbe Mikroanalytisches Laboratorium, Germany.

Cyclic voltammetry was recorded with an Autolab PGstat10 potentiostat controlled by GPES4 software under argon. A 3 mm diameter glassy carbon electrode was used as working electrode and plantuim as the counter electrode. The experimental reference was an Ag/AgCl electrode in the electrolyte solution (TBAP). Ferrocene was added at the end of each measurement as an internal standard. All electrode potentials reported in this publication are given versus the potential of the ferrocene/ferrocenium redox couple ($[Fc^{+/0}]$, $E^{o} = 0.00$ V) as the reference.

The apparent rate constant (k_{obs}) can be regarded as turn-over frequency (TOF) when a first-order or pseudo-first order H_2 evolving reaction is catalyzed by a freely diffusing molecular catalyst.[43] The corresponding equation is provided below: [7, 43]

$$\frac{i_c}{i_p} = \frac{n}{0.4463}\sqrt{\frac{RTk_{obs}}{Fv}}$$

Here, i_c is the maximum current of the catalytic peak, and i_p is the plateau current of the non-catalytic reduction wave. F is Faraday's constant, T is 295 K, R is the universal gas constant, v is the scan rate, n is 2 in the case of the H_2 evolution process.

3.4.3 Single crystal x-ray crystallography

All reflection intensities were measured at 110(2) K using a SuperNova diffractometer (equipped with Atlas detector) with Mo *K*α radiation (λ = 0.71073 Å)) (**1a**) or Cu *K*α radiation (λ = 1.54178 Å) (**2a**, **2b**) under the program CrysAlisPro (Version 1.171.36.32 Agilent Technologies, 2013). The same program was used to refine the cell dimensions and for data reduction. The structure was solved with the program SHELXS-2013[48] and was refined on F^2 with SHELXL-2013.[48] Analytical numeric absorption corrections based on a multifaceted crystal model were applied using CrysAlisPro. The temperature of the data collection was controlled using the system Cryojet (manufactured by Oxford Instruments). The H atoms were placed at calculated positions (unless otherwise specified, see below) using the instructions AFIX 23 or AFIX 43 with isotropic displacement parameters having values 1.2 times *U*eq of the attached C atoms.

1a: The H atoms attached to O1W and O2W (*i.e.*, lattice water molecules) were found from difference Fourier maps, and their coordinates were refined freely. The structure is ordered. The crystal lattice also contains some amount of very disordered solvent molecules. Their contribution has been taken out using the SQUEEZE procedure[49] in the final refinement.

2a: The H atoms attached to O1W, O2W (O2W is found at sites of twofold axial symmetry) and O3W were found from difference Fourier maps, and their coordinates were refined freely. The H atoms attached to the lattice water solvent molecules O3W' (minor component of the disordered water lattice molecule) and O4W (partially occupied with occupancy factor = 0.292(9)) could not be retrieved from difference Fourier maps. The structure is partly disordered. One part of the Ni complex and one lattice water solvent molecule (O3W/O3W') is disordered over two orientations, and the occupancy factors of the major components of the disorder refine to 0.649(11) and 0.861(4), respectively. One of the two counterions (Br2) is disordered over three orientations, and the occupancy factors of the three components refine to 0.779(2), 0.180(2) and 0.0410(8).

2b: The structure is ordered, except for some amount of disordered lattice solvent molecules, whose contribution has been taken out using the SQUEEZE procedure[49] in the final refinement.

3.4.4 ligand precursors synthesis

H_2**L1**Br_2 and H_2**L2**Br_2[28] were synthesized following literature methods with small modifications.

*H_2**L1**Br_2*:
N-Pyridylmethylbenzimidazole (4 mmol, 0.836 g) and α,α′-dibromo-o-xylene (2 mmol, 0.57 g) were added into a 25 ml round-bottomed flask containing 10 ml toluene. The mixture was stirred for 24 h at 110 °C, after which time the product was collected by filtration. The white powder was washed with THF and ether, and dried under vacuum. Yield: 1.32g (97%). ^{1}H NMR (300 MHz, DMSO-d_6) δ = 10.07 (s, 2H, NC*H*N), 8.48 (d, *J* = 4.77 Hz, 2H, Ar-*H*), 8.04 (s, 1H, Ar-*H*), 8.02 (d, *J* = 3.17 Hz, 2H, Ar-*H*), 7.98 (d, *J* = 2.60 Hz, 1H, Ar-*H*), 7.95 (t, *J* = 2.18, 2.18 Hz, 2H, Ar-*H*), 7.92 (d, *J* = 1.74 Hz, 1H, Ar-*H*), 7.90 (d, *J* = 1.76 Hz, 1H, Ar-*H*), 7.74 (s, 1H, Ar-*H*), 7.72 (s, 1H, Ar-*H*), 7.66 (m, 4H, Ar-*H*), 7.44 (dd, *J* = 3.33, 5.70 Hz, 2H, Ar-*H*), 7.38 (dd, *J* = 5.35, 7.05 Hz, 2H, Ar-*H*), 7.19 (dd, *J* = 3.46, 5.58 Hz, 2H, Ar-*H*), 6.16 (s, 2H, N-CH_2-Py), 6.00 (s, 2H, NCH_2). ^{13}C NMR (75 MHz, DMSO-d_6) δ = 152.87, 149.55, 148.05, 143.87, 137.58, 132.06, 131.55, 131.07, 129.37, 128.25, 127.07, 126.80, 123.74, 122.77, 114.07, 50.85, 47.53. ESI-MS found (calculated): $[M–2Br]^{2+}$ *m/z* 261.3 (261.1); $[M–Br]^+$ *m/z* 601.1 (601.2).

*H_2**L2**Br_2*:
N-Pyridylmethylimidazole (4 mmol, 0.836 g) and α,α′-dibromo-o-xylene (2 mmol, 0.57 g) were added into a 25 ml round-bottomed flask containing 10 ml toluene. The mixture was stirred for 48 h at 110 °C, after which time the product was collected by filtration. The sticky solid was crushed and washed with THF until it became a brown powder, which was dried under vacuum. Yield: 0.90 g (76%). ^{1}H NMR (300 MHz, DMSO-d_6) δ = 9.48 (s, 2H, NC*H*N), 8.55 (d, *J* = 4.6 Hz, 2H, Ar-*H*), 7.93 (d, *J* = 1.5 Hz, 1H, Ar-*H*), 7.91 (d, *J* = 1.2 Hz, 1H, Ar-*H*), 7.88 (s, 2H, Ar-*H*), 7.82 (s, 2H, Ar-*H*), 7.55 (d, *J* = 8.1 Hz, 2H, Ar-*H*), 7.52 – 7.48 (m, 2H, Ar-*H*), 7.41 (dd, *J* = 4.8, 2.1 Hz, 2H, Ar-*H*), 7.32 (dd, *J* = 3.48, 5.44 Hz, 2H, Ar-*H*), 5.73 (s, 4H, N-CH_2-Py), 5.64 (s, 4H, NCH_2). ^{13}C NMR (75 MHz, DMSO-d_6) δ = 153.41, 149.57, 137.54, 137.48, 132.98, 129.64, 129.38, 123.75, 123.70, 122.69, 122.56, 53.09, 49.12. ESI-MS found (calculated): $[M–2Br]^{2+}$ *m/z* 211.2 (211.6); $[M–Br]^+$ *m/z* 501.0 (502.1)

3.4.4 complexes synthesis

*Synthesis of [Ni(**L1**)Br]Br (**1a**) and [Ni(**L2**)]Br_2 (**2a**)*
Tetrabutylammonium bromide (2 g), nickel acetate (0.18 g, 1 mmol) and H_2**L1**Br_2 (0.69 g, 1 mmol) or nickel acetate (0.15 g, 0.84 mmol) and H_2**L2**Br_2 (0.49 g, 0.84 mmol) were weighed into a 10 ml round-bottomed flask. The mixture was heated at 80 °C under vacuum for 3 h. Then the temperature was increased to 120-130 °C and the flask was heated for another 24 h under vacuum. After cooling to room temperature the residue was triturated with 50 ml distilled water, and kept overnight. The mixture was filtered yielding a yellow powder. The powder was thoroughly washed with diethyl ether. Yield: **1a** 0.55 g (74%), **2a** 0.29 g (45%). Single crystals were obtained by the liquid-liquid diffusion method (MeCN/ether).

1a ^{1}H NMR (300 MHz, DMSO-d_6) δ = 8.49 (d, *J* = 5.50 Hz, 2H, Ar-*H*), 8.13 (m, 6H, Ar-*H*), 7.885 (dd, *J* = 3.66, 5.20 Hz, 2H, Ar-*H*), 7.34 – 7.44 (m, 10H, Ar-*H*), 7.25 (t, *J* = 7.70, 7.70

Hz, 2H, N-CH*H*-Py), 6.465 (d, *J* = 15.22 Hz, 2H, N-C*H*H-Py), 5.45 (d, *J* = 16.06 Hz, 2H, NCH*H*), 5.32 (d, *J* = 15.93 Hz, 2H, NC*H*H). ^{13}C NMR (75 MHz, DMSO-d_6) δ = 168.43, 154.56, 153.16, 141.00, 134.30, 134.04, 132.86, 132.78, 128.81, 124.81, 124.64, 124.34, 124.04, 112.77, 111.35, 50.76, 50.12. ESI-MS found (calculated): $[M–2Br]^{2+}$ *m/z* 289.0 (289.1); $[M–Br]^{+}$ *m/z* 657.1 (657.1). Anal. Calcd for Ni $C_{34}H_{28}N_6Br_2 \cdot 0.5H_2O \cdot 0.7CH_3CN$: C 54.83, H 4.18, N 11.64; found C 54.57, H 3.93, N 11.80.

2a ^{1}H NMR (300 MHz, DMSO-d_6) δ = 8.30 (d, *J* = 5.27 Hz, 2H, Ar-*H*), 8.11 (t, *J* = 7.62, 7.62 Hz, 2H, Ar-*H*), 7.88 (d, *J* = 7.62 Hz, 2H, Ar-*H*), 7.71 (d, *J* = 1.56 Hz, 2H, Ar-*H*), 7.55 (m, 2H, Ar-*H*), 7.35 – 7.37 (m, 4H, Ar-*H*), 6.98 (m, Ar-*H,* 4H, N-C*H*H-Py), 5.81 (d, *J* = 14.99 Hz, 2H, N-C*H*H-Py), 5.01 (d, *J* = 15.46 Hz, 2H, NCH*H*), 4.69 (d, *J* = 15.30 Hz, 2H, NC*H*H). ^{13}C NMR (75 MHz, DMSO-d_6) δ = 155.56, 154.67, 152.64, 140.83, 135.54, 131.42, 129.04, 124.97, 124.84, 124.67, 122.80, 53.39, 51.50. ESI-MS found (calculated): $[M–2Br]^{2+}$ *m/z* 239.1 (239.1); $[M–Br]^{+}$ *m/z* 557.0 (557.1). Anal. Calcd for $NiC_{26}H_{24}N_6Br_2 \cdot H_2O$: C 47.53, H 3.99, N 12.79; found C 47.73, H 3.74, N 12.69.

*[Ni(**L1**)](PF$_6$)$_2$ (**1b**) and [Ni(**L2**)](PF$_6$)$_2$ (**2b**)*

NH_4PF_6 (128 mg, 0.4 mmol) was dissolved in 15 ml methanol and the solution was brought to a boil. The compounds **1a** (74 mg, 0.1 mmol) or **2a** (64 mg, 0.1 mmol) were added into this boiling methanol solution. The resulting suspension was stirred for 30 min during which time it cooled down. The product was collected by filtration and the pale yellow solid was washed with cold methanol and diethyl ether. Yield: **1b** 35 mg (55%), **2b** 55 mg (72%). Single crystals were obtained by the liquid-liquid diffusion method (MeCN/ether).

1b ^{1}H NMR (300 MHz, DMSO-d_6) δ = 8.42 (s, *J* = 5.26 Hz, 2H, Ar-*H*), 8.15 – 8.18 (m, 5H, Ar-*H*), 7.87 (dd, *J* = 3.61, 5.23 Hz, 2H, Ar-*H*), 7.40 – 7.46 (m, 6H, Ar-*H*), 7.37 (s, 1H, Ar-*H*), 7.27 (m, 2H, Ar-*H*), 7.02 (d, *J* = 15.23 Hz, 2H, N-CH*H*-Py), 6.43 (d, *J* = 15.32 Hz, 2H, N-C*H*H-Py), 5.48 (d, *J* = 15.99 Hz, 2H, NCH*H*), 5.17 (d, *J* = 15.83 Hz, 2H, NC*H*H). ^{13}C NMR (75 MHz, DMSO-d_6) δ = 168.11, 154.54, 152.65, 141.23, 134.23, 132.89, 132.76, 128.82, 124.97, 124.89, 124.40, 124.06, 112.86, 111.42, 101.22, 50.41, 49.89. ^{31}P NMR (122 MHz, DMSO-d_6) δ = –144.88. ESI-MS found (calculated): $[M–2PF_6]^{2+}$ *m/z* 289.9 (289.9); $[M–PF_6]^{+}$ *m/z* 723.2 (723.1). Anal. Calcd for $NiC_{34}H_{28}N_6(PF_6)_2 \cdot CH_3CN$: C 47.50, H 3.43, N 10.77; found C 47.78, H 3.43, N 10.80.

2b ^{1}H NMR (300 MHz, DMSO-d_6) δ = 8.25(d, *J* = 15.99 Hz, 2H, Ar-*H*), 8.12 (t, *J* = 7.41, 7.41 Hz, 2H, Ar-*H*), 7.89 (d, *J* = 7.57 Hz, 2H, Ar-*H*), 7.71 (s, 2H, Ar-*H*), 7.54 (m, 2H, Ar-*H*), 7.40 – 7.46 (m, 4H, Ar-*H*), 6.99 (s, 2H, Ar-*H*), 6.77 (d, *J* = 14.93 Hz, 2H, N-CH*H*-Py), 5.80 (d, *J* = 15.01 Hz, 2H, N-C*H*H-Py), 5.04 (d, *J* = 15.39 Hz, 2H, NCH*H*), 4.61 (d, *J* = 15.26 Hz, 2H, NC*H*H). ^{13}C NMR (75 MHz, DMSO-d_6) δ = 155.45, 154.62, 152.33, 141.01, 135.47, 131.44, 129.10, 125.17, 124.99, 124.88, 122.93, 53.28, 51.34. ^{31}P NMR (122 MHz, DMSO-d_6) δ = –144.87. ESI-MS found (calculated): $[M–2PF_6]^{2+}$ *m/z* 239.1 (239.6). Anal. Calcd for $NiC_{26}H_{24}N_6(PF_6)_2$: C 40.60, H 3.15, N 10.93; found C 40.64, H 3.18, N 10.92.

3.5 Acknowledgements

S. Luo gratefully acknowledges a grant from the Chinese Scholarship Council (no. 201306410011). We are grateful to Mr. John van Dijk for mass spectrometry.

3.6 Reference

[1] P.D. Tran, J. Barber, *Phys. Chem. Chem. Phys.* 2012, 14, 13772-13784.
[2] J.D. Holladay, J. Hu, D.L. King, Y. Wang, *Catal. Today* 2009, 139, 244-260.
[3] V. Khrizanforova, I. Knyazeva, V. Matveeva Sokolova, I. Nizameev, T. Gryaznova, M. Kadirov, A. Burilov, O. Sinyashin, Y. Budnikova, *Electrocatalysis* 2015, 6, 357-364.
[4] A. Lewandowska-Andralojc, T. Baine, X. Zhao, J.T. Muckerman, E. Fujita, D.E. Polyansky, *Inorg. Chem.* 2015, 54, 4310-4321.
[5] N. Queyriaux, R.T. Jane, J. Massin, V. Artero, M. Chavarot-Kerlidou, *Coord. Chem. Rev.* 2015, 304-305, 3-19.
[6] S. Canaguier, V. Fourmond, C.U. Perotto, J. Fize, J. Pecaut, M. Fontecave, M.J. Field, V. Artero, *Chem. Commun.* 2013, 49, 5004-5006.
[7] L. Gan, T.L. Groy, P. Tarakeshwar, S.K.S. Mazinani, J. Shearer, V. Mujica, A.K. Jones, *J. Am. Chem. Soc.* 2015, 137, 1109-1115.
[8] D.L. DuBois, R.M. Bullock, *Eur. J. Inorg. Chem.* 2011, 1017-1027.
[9] M.T.M. Koper, E. Bouwman, *Angew. Chem. Int. Ed.* 2010, 49, 3723-3725.
[10] S.M. Laga, J.D. Blakemore, L.M. Henling, B.S. Brunschwig, H.B. Gray, *Inorg. Chem.* 2014, 53, 12668-12670.
[11] L. Tong, R. Zong, R.P. Thummel, *J. Am. Chem. Soc.* 2014, 136, 4881-4884.
[12] D. Basu, S. Mazumder, X. Shi, H. Baydoun, J. Niklas, O. Poluektov, H.B. Schlegel, C.N. Verani, *Angew. Chem. Int. Ed.* 2015, 54, 2105-2110.
[13] R.M. Stolley, J.M. Darmon, M.L. Helm, *Chem. Commun.* 2014, 50, 3681-3684.
[14] M. van der Meer, E. Glais, I. Siewert, B. Sarkar, *Angew. Chem. Int. Ed.* 2015, 54, 13792-13795.
[15] J. Berding, T.F. van Dijkman, M. Lutz, A.L. Spek, E. Bouwman, *Dalton Trans.* 2009, 6948-6955.
[16] L.P. Bheeter, M. Henrion, L. Brelot, C. Darcel, M.J. Chetcuti, J.-B. Sortais, V. Ritleng, *Adv. Synth. Catal.* 2012, 354, 2619-2624.
[17] E.A. Bielinski, W. Dai, L.M. Guard, N. Hazari, M.K. Takase, *Organometallics* 2013, 32, 4025-4037.
[18] K. Fuji, S. Tamba, K. Shono, A. Sugie, A. Mori, *J. Am. Chem. Soc.* 2013, 135, 12208-12211.
[19] P. Guan, C. Cao, Y. Liu, Y. Li, P. He, Q. Chen, G. Liu, Y. Shi, *Tetrahedron Lett.* 2012, 53, 5987-5992.
[20] L. Postigo, B. Royo, Adv. *Synth. Catal.* 2012, 354, 2613-2618.
[21] Z. Xi, X. Zhang, W. Chen, S. Fu, D. Wang, *Organometallics* 2007, 26, 6636-6642.
[22] Z. Xi, B. Liu, W. Chen, *J. Org. Chem.* 2008, 73, 3954-3957.
[23] M.C. Jahnke, T. Pape, F.E. Hahn, *Eur. J. Inorg. Chem.* 2009, 1960-1969.
[24] M.H. Reineke, M.D. Sampson, A.L. Rheingold, C.P. Kubiak, *Inorg. Chem.* 2015, 54, 3211-3217.
[25] V.S. Thoi, C.J. Chang, *Chem. Commun.* 2011, 47, 6578-6580.

[26] V.S. Thoi, N. Kornienko, C.G. Margarit, P. Yang, C.J. Chang, *J. Am. Chem. Soc.* 2013, 135, 14413-14424.
[27] J. Dinda, S.D. Adhikary, S.K. Seth, A. Mahapatra, *New J. Chem.* 2013, 37, 431-438.
[28] J. Berding, M. Lutz, A.L. Spek, E. Bouwman, *Organometallics* 2009, 28, 1845-1854.
[29] Q.-X. Liu, Z.-Q. Yao, X.-J. Zhao, Z.-X. Zhao, X.-G. Wang, *Organometallics* 2013, 32, 3493-3501.
[30] A.W. Addison, T.N. Rao, J. Reedijk, J. Vanrijn, G.C. Verschoor, *J Chem Soc-Dalton Trans.* 1984, 1349-1356.
[31] R. Garcia-Bueno, M.D. Santana, G. Sanchez, J. Garcia, G. Garcia, J. Perez, L. Garcia, *Dalton Trans.* 2010, 39, 5728-5736.
[32] E.I. Musina, V.V. Khrizanforova, I.D. Strelnik, M.I. Valitov, Y.S. Spiridonova, D.B. Krivolapov, I.A. Litvinov, M.K. Kadirov, P. Lonnecke, E. Hey-Hawkins, Y.H. Budnikova, A.A. Karasik, O.G. Sinyashin, *Chem. -Eur. J.* 2014, 20, 3169-3182.
[33] M.D. Santana, A.A. Lozano, G. Garcia, G. Lopez, J. Perez, *Dalton Trans.* 2005, 104-109.
[34] H. Ma, S. Chattopadhyay, J.L. Petersen, M.P. Jensen, *Inorg. Chem.* 2008, 47, 7966-7968.
[35] H. Ma, J.L. Petersen, V.G. Young, G.T. Yee, M.P. Jensen, *J. Am. Chem. Soc.* 2011, 133, 5644-5647.
[36] S.F. Tyler, S.N. Natoli, B. Vlaisavljevich, P.E. Fanwick, T. Ren, *Inorg. Chem.* 2015, 54, 10058-10064.
[37] J.-i. Nishigaki, T. Matsumoto, K. Tatsumi, *Eur. J. Inorg. Chem.* 2010, 5011-5017.
[38] L. Yang, D.R. Powell, R.P. Houser, *Dalton Trans.* 2007, 955-964.
[39] E.C.M. Ording-Wenker, M.A. Siegler, M. Lutz, E. Bouwman, *Inorg. Chem.* 2013, 52, 13113-13122.
[40] M. Sheng, N. Jiang, S. Gustafson, B. You, D.H. Ess, Y. Sun, *Dalton Trans.* 2015, 44, 16247-16250.
[41] J. Heinze, *Angew. Chem. Int. Ed.* 1984, 23, 831-847.
[42] V. Fourmond, S. Canaguier, B. Golly, M.J. Field, M. Fontecave, V. Artero, *Energy Environ Sci.* 2011, 4, 2417-2427.
[43] P. Zhang, M. Wang, Y. Yang, T. Yao, L. Sun, *Angew. Chem.* 2014, 53, 13803-13807.
[44] V. Fourmond, P.-A. Jacques, M. Fontecave, V. Artero, *Inorg. Chem.* 2010, 49, 10338-10347.
[45] M.P. Stewart, M.-H. Ho, S. Wiese, M.L. Lindstrom, C.E. Thogerson, S. Raugei, R.M. Bullock, M.L. Helm, *J. Am. Chem. Soc.* 2013, 135, 6033-6046.
[46] R. Tatematsu, T. Inomata, T. Ozawa, H. Masuda, *Angew. Chem. Int. Ed.* 2016, 55, 5247-5250.
[47] K. Kawano, K. Yamauchi, K. Sakai, *Chem. Commun.* 2014, 50, 9872-9875.
[48] G.M. Sheldrick, *Acta Cryst. A* 2008, 64, 112-122.
[49] A.L. Spek, *Acta Cryst. D* 2009, 65, 148-155.